

Fabrication and Optimization of Chloride Ion electrode based on bilayer membrane

Zhe Li¹, Huang Shunhao¹, Juan Chen^{1,*}, Zhuang Junpeng²

¹ College of Information Science and Technology, Beijing University of Chemical Technology, Beijing 100029, PR China

² College of Chemistry, Beijing University of Chemical Technology, Beijing 100029, PR China

*E-mail: jchen@mail.buct.edu.cn

Received: 14 March 2020 / Accepted: 13 April 2020 / Published: 10 June 2020

Bilayer membrane electrode is an effective method to improve the performance of traditional ion select electrode. By adjusting the composition of the membrane, the ion flux in the electrode membrane is controlled, thus the detection performance of the electrode can be changed. With the help of least square support vector machine and orthogonal experiment, the electrode model was established with the membrane thickness and ion exchanger concentration as factors, and the optimal parameters of the model were applied to the chloride ion PVC membrane electrode. The experimental results show that the detection limit of bilayer chloride ion electrode is one order of magnitude lower than that of traditional membrane electrode.

Keywords: Chloride quantification, Electrochemistry, Bilayer membrane, Orthogonal experiment, Support vector machine

1. INTRODUCTION

Chloride ion, as a common and important anion, widely exists in various fields such as environment, food, biology, medical treatment and industry [1-5]. Especially in the industrial field, chloride ions may cause corrosion of copper, aluminum and even stainless steel [6-8], and may threaten the safe use of boiler or turbine blades [9-11]. Ion chromatography, fluorescence spectrometry and flow injection method can meet the requirements for the measurement of trace chloride ions, but these methods may have some measurement delay [12-13]. The ion selective electrode (ISE) based on polymer membrane can measure chloride ion rapidly and continuously, however, the detection limit of chloride ion membrane ISE, as far as we known, is about $10^{-5.5}$ M [5,14], which impedes the application of the ISE method on chloride measurement.

The performance and analytical parameters of the ISE depend on the composition of the membrane and the concentration of ionic components within it [15]. But these changes are not easy for chloride ions. After over 20 years of research, the mainstream chloride selective membrane is still composed of mercury organic ionophore, chloride quaternary ammonium salt ion exchanger, polyvinyl chloride (PVC) and plasticizer [16-19]. It is not easy to develop new ionophore and ion exchanger, at the same time, replacing PVC and plasticizers with acrylates is difficult because acrylates contain too many impurities that interfere with chloride ion measurements [20].

A few years ago, Michalska and co-workers introduced a new method called Potentiometric bilayer membrane. The performance of the ISE can be changed by careful tailoring the bilayer membrane made of poly (hexyl acrylate) and / or poly (lauryl acrylate) and different ion exchangers. By creating the ion flux between the inner membrane and the outer membrane, this concept reduces the ion accumulation at the interface between the outer membrane and the solution, so the detection limit of the bilayer membrane ISE is lower than that of the monolayer membrane [15,21]. This method has been verified on potassium and copper ion selective electrodes, but its effect on anion electrodes is unknown. In addition, the ion flux is affected by the membrane material, the type and concentration of the ion exchanger, the thickness of the membrane and other factors. How to design the bilayer membrane efficiently and accurately is also a problem to be solved. If the single variable method is used to solve this problem, not only the number of experiments is very large, but also the relationship between different factors may be ignored in the single variable experiment. Central composite design, box behnken and response surface methodology have been successfully used to optimize the design of polymer membranes for ion selective electrodes [22-23]. When there are four experimental factors, this method needs 27 groups of experiments to ensure the accuracy of the model. The previous research of our group shows that the number of experimental groups can be further compressed to 9 by using orthogonal experiment and least square support vector machine (LS-SVM) to establish the optimization model, and the excellent prediction effect can be obtained [24]. However, this method has not been used to optimize the membrane ISE, and the optimization effect of the bilayer membrane is still unknown.

In this paper, the bilayer PVC membrane chloride ion ISE was fabricated and investigated. Two different kinds of lipid soluble quaternary ammonium salt were used as the ion exchangers to control the ion flux. The orthogonal experiment was designed with membrane thickness and ion exchanger concentration as factors. The prediction models of bilayer membrane electrode parameter and membrane structure were established by LS-SVM method. The impact of structure on the performance was analysed by using the contours of the prediction model, and the optimal parameter range was obtained. To the best of our knowledge, both the bilayer PVC membrane chloride ion ISE and the optimization model of bilayer membrane have never report before.

2. MATERIALS AND EXPERIMENTAL

2.1. Materials

The chloride ionophore III (ETH9033), tridodecylmethylammonium chloride (TDMACl), poly (3-hexylthiophene-2,5-diyl) (POT) and high molecular weight poly (vinyl chloride) (PVC) were provi

ded by Sigma-Aldrich. Sodium chloride in working chemical grade was provided by Beijing Chemical Works. Bis (2-ethylhexyl)sebacate (DOS), tetrahydrofuran (THF), sodium hydrogencarbonate and other materials in analytical-reagent grade were provided by Sinopharm Chemical Reagent. Deionized water (conductivity = $0.055 \mu\text{Scm}^{-1}$) was produced by Millipore ultrapure water system (ADVANTAGE A10).

2.2. Instrument and equipment

Unless otherwise specified, the electrochemical experiments in this work were carried out at a constant temperature of $25 \text{ }^\circ\text{C}$ by using refrigerated circulators (HAAKE Arctic A10 Thermo Fisher Scientific).

The potential responses of all electrodes were measured synchronously by using a 6 1/2-digit (22-bit) data acquisition unit (Agilent 34970A) equipped with a 20-channel multiplexer module (Agilent 34901A). An Ag/AgCl double junction electrode was used as the reference electrode, in which the inner salt bridge was 3 M KCl, and the outer salt bridge was 0.1 M LiAc. The liquid junction potential and activity coefficient were calculated by Henderson equation and Debye–Hückel equation, respectively.

The electrochemical impedance test was carried out in a conventional three-electrode electrode cell. The reference electrode is same as the electrode used in the potential test, which is the Ag/AgCl (3 M KCl) double-junction electrode, the auxiliary electrode was a platinum wire, and the electrolyte is 0.1 M KCl solution. The frequency range of electrochemical impedance measurement was 20 mHz-10 KHz with a 10 mV sine wave excitation signal.

2.3. Electrode preparation

2.3.1. Indicator electrodes and solid contacts

The glassy carbon electrode with a surface area of 0.07 cm^2 was polished by 0.3 and $0.05 \mu\text{m}$ powder successively, and then cleaned by ultrasonic wave alternately in acetone and water. POT was dissolved in chloroform with a concentration of 6 mg/ml. As the solid contact layer, 10 μl of the solution was applied by drop casting on each glassy carbon electrodes and dry naturally.

2.3.2. Ion-selective membranes and electrode fabrication

In order to control the ion flux, three membrane solutions with different concentration of ion exchanger were prepared. The polymer membrane components including chloride ionophore III (2.0 wt.%), TDMACl (0.2, 0.5, 0.8 wt.%, corresponding ion concentration is 3.4, 8.5, 13.5 mol/m^3), PVC (33 wt.%) and DOS (64.8, 64.5, 64.2 wt.%). All components were dissolved in THF (dry mass = 13.65%). Thickness of outer layer, ion exchanger concentration in outer layer, thickness of inner layer and ion exchanger concentration in inner layer were selected as experimental factors of the orthogonal experimental design (OED), and each factor had three levels. As shown in the Table 1, these factors

may affect the ion flux of the bilayer membrane electrode and further affect the detection performance of the electrode. The electrode are divided into 10 different configurations, as shown in Table 2, the first 9 configurations are consistent with a typical OED table of L9 (3^4) because it could be used to study 4 factors. As a comparison, the No.10 configuration is added, which has no inner layer and is used as a typical representative of the traditional monolayer electrode. According to the configuration in Table 2, firstly, the inner membrane solution was applied on the surface of the electrode and kept vertical for over 24 hours until the film is completely dry. By conditioned in 0.1M sodium bicarbonate solution, the TDMACl in the inner membrane was converted to tridodecylmethylammonium hydrogen carbonate (TDMAHCO₃) through ion exchange (The calculation of soaking time will be discussed in subsequent section 3.1), which has been previously confirmed by Lewenstam et al[25]. After soaking, the electrode was left standing for an additional 96 h to make the concentration of bicarbonate ion in the membrane as uniform as possible. Finally, the outer membrane of the electrode was applied on the inner membrane by drip coating, and TDMAHCO₃ was fixed in the inner membrane, which could not directly contact with the solution under test, and the ion flux flowing from the outer membrane to the inner membrane was formed.

Table 1. Factors and levels of OED.

Level	Factors			
	A (outer layer thickness)(μm)	B (outer layer ion exchanger concentration) (mol/m^3)	C (inner layer thickness) (μm)	D (inner layer ion exchanger concentration) (mol/m^3)
1	25	3.4	25	3.4
2	50	8.5	50	8.5
3	75	13.5	75	13.5

Table 2. Experimental design table

Test No.	Factors level			
	A(μm)	B(mol/m^3)	C(μm)	D(mol/m^3)
1	1	1	1	1
2	2	2	2	1
3	3	3	3	1
4	3	2	1	2
5	2	1	3	2
6	1	3	2	2
7	1	2	3	3
8	2	3	1	3
9	3	1	2	3
10	2	2	-	-

2.4 Theoretical

In 0.1M sodium bicarbonate solution, bicarbonate ions enter the inner layer due to diffusion and electromigration, and reacts with TDMACl to form TDMAHCO₃. The total amount of ions entering the membrane can be controlled by the soaking time. Affected by the thickness and composition of the inner layer membrane, the soaking time of the electrode in sodium bicarbonate solution is different. In order to estimate the diffusion time of hydrogen carbonate ions in the inner

layer, the ion diffusion model of the inner layer was established by using the finite difference method. The one-dimensional ion flux in the liquid phase can be expressed by the following equation [26]:

$$J_i(x,t) = -D_i \frac{\partial c_i}{\partial x} - \frac{z_i F}{RT} c_i D_i \frac{\partial E}{\partial x} + c_i v(x) \tag{1}$$

$$\frac{\partial c_i}{\partial t} = -\frac{\partial J_i}{\partial x} \tag{2}$$

Equation (1) can be rewritten by using the potential function $\Psi = \frac{FE}{RT}$:

$$J_i(x,t) = -D_i \frac{\partial c_i}{\partial x} - z_i c_i D_i \frac{\partial \Psi}{\partial x} + c_i v(x) \tag{3}$$

Where $J_i(x)$, D_i , c_i , x , z_i , $v(x)$ represent the the ion flux in x-direction, the diffusion coefficient, the ion concentration, the distance, the charge of the species and the flow velocity in x-direction respectively. F is the Faraday constant, R the universal gas constant, T the absolute temperature, E the electrical potential and t the time.

The inner layer is represented by N continuous thin segments with the thickness of δ , and the forward difference method is used to rewrite equation (3) and (2):

$$J_{i,v/v+1}(t) = \frac{D_i(c_{i,v} - c_{i,v+1})}{\delta} + \frac{0.5z_i D_i(c_{i,v} + c_{i,v+1})(\Psi_v - \Psi_{v+1})}{\delta} + 0.5(c_{i,v} + c_{i,v+1})v \tag{4}$$

$$\frac{c_{i,v}(t + \Delta t) - c_{i,v}(t)}{\Delta t} = \frac{J_{i,v-1}(t) - J_{i,v/v+1}(t)}{\delta} \tag{5}$$

Where $J_{i,v/v+1}(t)$ is the ion flux from the v segment to $v+1$ segment, c_i is replaced by $0.5(c_{i,v} + c_{i,v+1})$ that indicate the concentration of each segment, and Δt is the time interval.

By combining equations (4) and (5), the following equations describing the change of concentration can be derived:

$$\begin{aligned} c_{i,v}(t + \Delta t) = c_{i,v}(t) + \frac{\Delta t}{\delta} & \left(\frac{D_i(c_{i,v-1} - 2c_{i,v} + c_{i,v+1})}{\delta} \right. \\ & + \frac{0.5z_i D_i(c_{i,v-1} + c_{i,v})(\Psi_{v-1} - \Psi_v)}{\delta} \\ & + \frac{0.5z_i D_i(c_{i,v} + c_{i,v+1})(\Psi_v - \Psi_{v+1})}{\delta} \\ & \left. + 0.5(c_{i,v-1} - c_{i,v+1})v \right) \end{aligned} \tag{6}$$

In order to simplify the previous equation so that it satisfies the traditional forward difference form, define:

$$\begin{cases} \tau = \frac{D_0}{\delta^2} t \\ w = \frac{\delta}{D_0} v \end{cases} \tag{7}$$

The value of diffusion coefficient D_0 is arbitrary constant, τ is the dimensionless time and w the dimensionless flow velocity. Equation (6) can be rewritten as:

$$\begin{aligned} c_{i,v}(\tau + \Delta \tau) = c_{i,v}(\tau) + \frac{D_i(c_{i,v-1} - 2c_{i,v} + c_{i,v+1})\Delta \tau}{D_0} \\ + \frac{0.5z_i D_i(c_{i,v-1} + c_{i,v})(\Psi_{v-1} - \Psi_v)\Delta \tau}{D_0} \\ + \frac{0.5z_i D_i(c_{i,v} + c_{i,v+1})(\Psi_v - \Psi_{v+1})\Delta \tau}{D_0} \\ + 0.5(c_{i,v-1} - c_{i,v+1})w\Delta \tau \end{aligned} \tag{8}$$

The interface potential can be described by Nernst equation as follows:

$$E_{v+1} - E_v = -\frac{RT}{z_i F} \cdot \ln \frac{a_{v+1}}{a_v} \tag{9}$$

Where a_v is the activity coefficient. In a dilute solution or solid phase, It can be considered that $a_i = c_i = 0.5(c_{i,d+1} + c_{i,d})$, equation (9) can be rewritten as:

$$\Psi_d - \Psi_{d+1} = \frac{1}{z_i} \ln \frac{(c_{i,d+1} + c_{i,d})}{(c_{i,d} + c_{i,d-1})} \tag{10}$$

Define $D_i = D_0$ and skip the targets related to the flow velocity, finally, the membrane concentration can be expressed by the equation as follows:

$$\begin{aligned} c_{i,d}(\tau + \Delta\tau) = & c_{i,d}(\tau) + (c_{i,d-1} - 2c_{i,d} + c_{i,d+1})\Delta\tau \\ & + 0.5(c_{i,d-1} + c_{i,d})\Delta\tau \ln \frac{(c_{i,d} + c_{i,d-1})}{(c_{i,d-1} + c_{i,d-2})} \\ & + 0.5(c_{i,d} + c_{i,d+1})\Delta\tau \ln \frac{(c_{i,d+1} + c_{i,d})}{(c_{i,d} + c_{i,d-1})} \end{aligned} \tag{11}$$

All calculations were carried out using Matlab 2016a (MathWorks).

3. RESULT AND DISCUSSION

3.1. Digital simulations

Using the forward difference method, based on equation (11), the concentration distribution of ions in the membrane with time and distance is analysed by numerical simulation. Assuming that the concentration of bicarbonate ion outside the membrane is 0.1 mol/L and the chloride ion is 0 mol/L, the concentration of bicarbonate ion outside the membrane does not change with time during the simulation process. The initial concentration of chloride ion in the membrane is 3.4, 8.5, 13.5 mol/m³, and the initial concentration of bicarbonate ion in the membrane is 0 mol/L. During the simulation, the total thickness of the membrane is 300 μm, which is composed of 200 small segments, each with a thickness of 1.5 μm. The total time is 40000 s, consisting of 1000 segments of 20 s each. Also assuming that the diffusion coefficients of bicarbonate ion and chloride ion are equal, it can be measured indirectly by telephone impedance method as follows [21]:

$$D_i = \frac{RTx}{AR_i F^2 \sum z_i^2 c_i} \tag{12}$$

Where A represents the electrode surface area, that is, 0.07 cm². R_i represents the low frequency resistance of electrochemical impedance spectroscopy. As a result, the diffusion coefficients of the inner membranes with chloride ion concentrations of 3.4, 8.5 and 13.5 mol/m³ were 1.27×10⁻¹³, 1.52×10⁻¹³ and 1.74×10⁻¹³ m²/s, respectively.

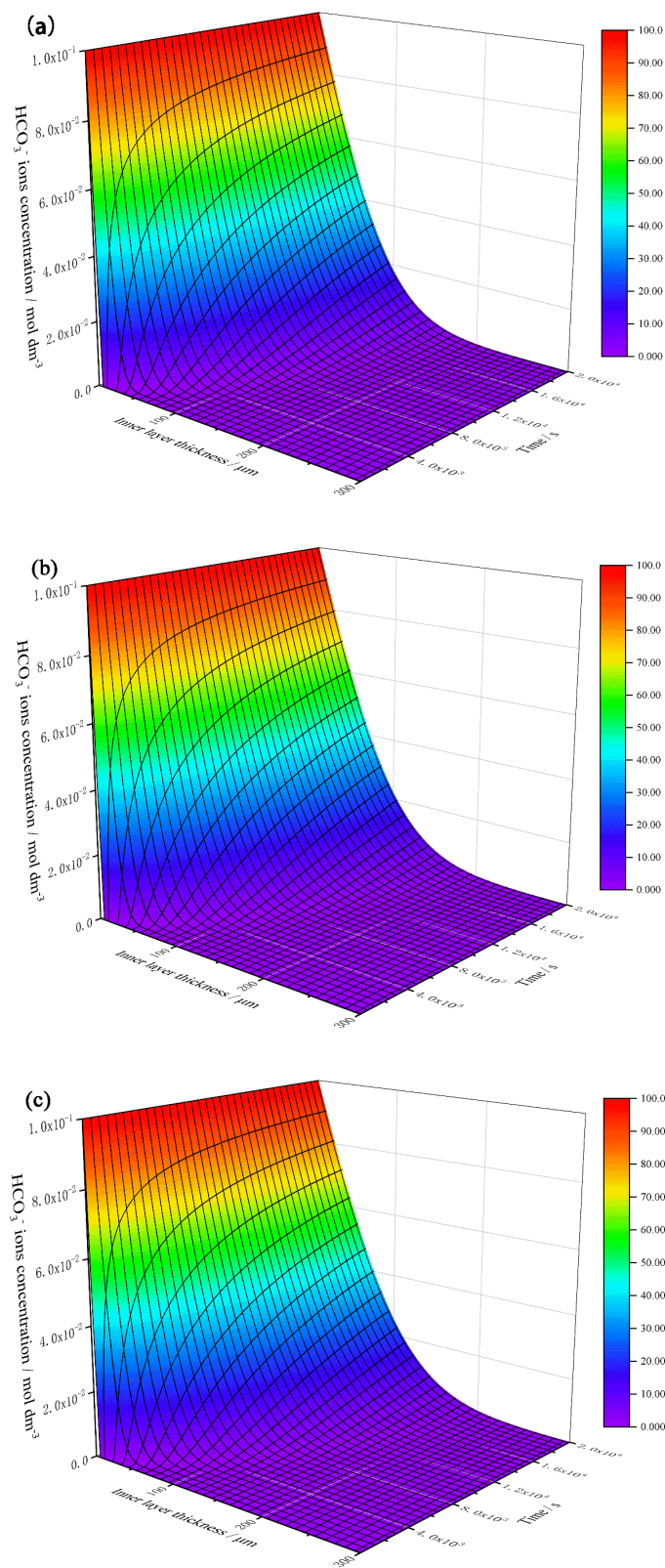


Figure 1. Simulated concentration profiles of bicarbonate ion in the membrane in 0.1mol/L sodium bicarbonate solution. (a) Membrane diffusion coefficient: $1.27 \times 10^{-13} \text{ m}^2/\text{s}$, initial chloride ion concentration: $3.4 \text{ mol}/\text{m}^3$. (b) Membrane diffusion coefficient: $1.52 \times 10^{-13} \text{ m}^2/\text{s}$, initial chloride ion concentration: $8.5 \text{ mol}/\text{m}^3$. (c) Membrane diffusion coefficient: $1.74 \times 10^{-13} \text{ m}^2/\text{s}$, initial chloride ion concentration: $13.5 \text{ mol}/\text{m}^3$.

The membrane used in the experiment contains three different initial chloride ion concentrations and diffusion coefficients, so three sets of concentration-time-distance surfaces are obtained by digital simulation, as shown in Fig.1. As can be seen from the figure, there does not seem to be much difference between the three surfaces because there is only a slight difference in the diffusion coefficients of the three membrane. At the position close to the solution in the membrane, the bicarbonate ion concentration will rise rapidly in a very short time, and gradually approach the ion concentration outside the membrane. On the contrary, the concentration of bicarbonate ion in the deep part of the membrane rises very slowly. The soaking time obtained by digital simulation is shown in Table 3.

Table 3. Digital simulation results of soaking time.

Ion concentration (mol/m ³)	Membrane thickness (μm)	Diffusion coefficient (m ² /s)	Soaking time (s)
3.4	25	1.27×10 ⁻¹³	52
3.4	50	1.27×10 ⁻¹³	97
3.4	75	1.27×10 ⁻¹³	147
8.5	25	1.52×10 ⁻¹³	103
8.5	50	1.52×10 ⁻¹³	230
8.5	75	1.52×10 ⁻¹³	401
13.5	25	1.74×10 ⁻¹³	152
13.5	50	1.74×10 ⁻¹³	383
13.5	75	1.74×10 ⁻¹³	717

3.2. Potentiometric calibration plots

The bilayer membrane electrode used in this study is made of two layers of PVC membrane with different ion concentration and thickness. The difference of diffusion coefficient, ion concentration and thickness may lead to the difference of ion flux and change the potential response of the electrode. Fig. 2 shows the potential calibration curves of 10 groups of electrodes in the Table 2. It can be seen from the curve that all the electrodes show good linearity in the region where the concentration is higher than 10⁻⁵ M even the slope of the electrode is not consistent. Compared with the No. 10 monolayer membrane electrode, the potential of the other 9 bilayer membrane electrodes is higher about 300 mV. This shows that there is an obvious interface between the two layers of PVC membrane, which leads to this obvious potential difference. The potential response characteristics of No. 1-9 bilayer membrane electrode were different when the concentration was lower than 10⁻⁵ M. The slope of most electrodes decreases, but the extent of the decrease seems to be smaller than that of monolayer electrode. Electrode No. 9 seems to have the best potential response, and its detection limit appears to be an order of magnitude lower than that of the monolayer. These results confirm that the potential response characteristic of bilayer membrane electrode is generally better than that of monolayer membrane electrode. After the precision tailoring of the electrode, the performance of the electrode will be further improved, which shows the necessity of optimizing the electrode parameters.

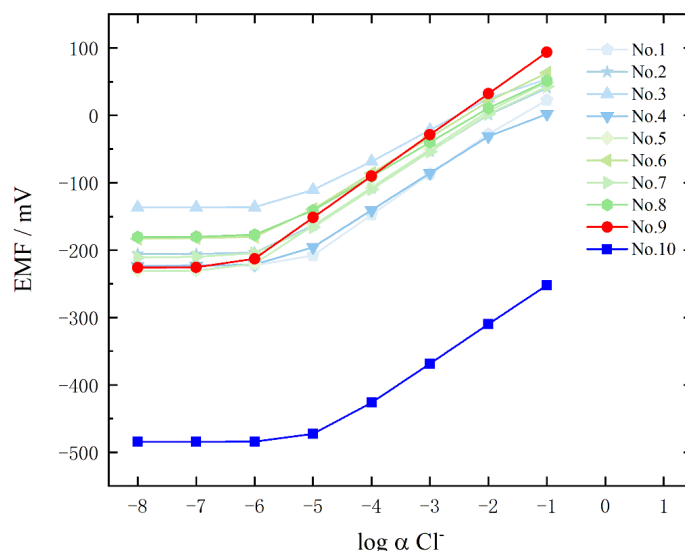


Figure 2. Potentiometric calibration plots for electrodes in Table 2. No. 1: pentagons, No. 2: five-pointed stars, No. 3: up triangles, No. 4: down triangles, No. 5: rhombuses, No. 6: left triangles, No. 7: right triangles, No. 8: hexagons, No. 9: circles, No. 10: squares.

3.3. Orthogonal experimental results

According to the orthogonal table $L_9 (3^4)$, the slope and detection limit (D_L) of bilayer membrane electrode was recorded, as shown in Table 4. The sum of slope or D_L in the same level i , corresponding average value k_i and range R were calculated respectively as follows:

$$k_i(\text{slope}) = \frac{\sum \text{slope}}{3}, i = 1, 2, 3 \tag{13}$$

$$k_i(D_L) = \frac{\sum D_L}{3}, i = 1, 2, 3 \tag{14}$$

$$R(\text{slope}) = k(\text{slope})_{\max} - k(\text{slope})_{\min} \tag{15}$$

$$R(D_L) = k(D_L)_{\max} - k(D_L)_{\min} \tag{16}$$

$k_i(\text{slope})$ represent the impact of level i of each factor to the slope, and $k_i(D_L)$ represent the impact of level i of each factor to the detection limit. The higher the k_i is, the higher the slope is, and the lower the detection limit is. R indicates the impact of each factor on the slope or detection limit, and a higher R value means that the factor has a greater impact on the slope or detection limit. For the slope of the bilayer membrane electrode, as can be seen from the orthogonal table, the order of range was $R_B > R_C > R_A > R_D$. According to the R value, the impact of the four factors on the slope decreases in the order of $B > C > A > D$. The optimal combination is $A_1B_1C_2D_3$. Similarly, the detection limit for bilayer membrane electrodes, the order of range was $R_C = R_D > R_B > R_A$. According to the R value, the impact of the four factors on the slope decreases in the order of $C = D > B > A$. The optimal combination is $A_2B_1C_2D_3$. Comparing the two groups of orthogonal results, A play the smallest role for both Slope and D_L , and B, C, D is the major impact factor. However, there are obvious differences

in the impact of factors on the slope and detection limit. The outer layer ion concentration and inner layer thickness have a greater influence on the electrode slope, while the inner layer thickness and inner layer ion concentration have greater influence on the electrode detection limit. The outer layer thickness is the minimum factor for both the slope and the detection limit.

Table 4. Results of orthogonal experiment design and range analysis of slope and detection limit.

Test No.	Factors				Slope(mV/dec)	D _L (lgα)
	A(μm)	B(mol/m ³)	C(μm)	D(mol/m ³)		
1	1	1	1	1	60.0	-5.4
2	2	2	2	1	54.7	-5.6
3	3	3	3	1	45.1	-5.4
4	3	2	1	2	54.9	-5.5
5	2	1	3	2	56.7	-6.1
6	1	3	2	2	53.3	-5.7
7	1	2	3	3	56.0	-5.8
8	2	3	1	3	50.6	-5.7
9	3	1	2	3	61.2	-6.2
k ₁ (slope)	56.44	59.33	55.17	53.26		
k ₂ (slope)	54.00	55.18	57.54	54.97		
k ₃ (slope)	53.72	49.66	51.46	55.94		
R(slope)	2.72	9.68	6.09	2.69		
order(slope)	R _B >R _C >R _A >R _D					
Optimal level(slope)	A ₁	B ₁	C ₂	D ₃		
Optimal combination(slope)	A ₁ B ₁ C ₂ D ₃					
k ₁ (D _L)	5.63	5.90	5.53	5.47		
k ₂ (D _L)	5.80	5.63	5.97	5.77		
k ₃ (D _L)	5.70	5.60	5.63	5.90		
R(D _L)	0.17	0.30	0.43	0.43		
order(D _L)	R _C =R _D >R _B >R _A					
Optimal level(D _L)	A ₂	B ₁	C ₂	D ₃		
Optimal combination(D _L)	A ₂ B ₁ C ₂ D ₃					

3.4. The establishment of electrode performance prediction model

The orthogonal experiment can be carried out according to the typical factors and levels within the scope of the experiment to reduce the number of experiments. It is a simple and effective method to obtain the optimal combination of orthogonal experiments by using corresponding average value k_i and range R . The orthogonal experiment simplifies the global experiment and tells us the level at which each factor affects the performance of the electrode. However, the results of orthogonal experiments are semi-quantitative and simple, which makes it impossible to give an accurate optimal value. Using the data of the orthogonal experiment obtained in this study, the prediction model is established by

using the LS-SVM method, which can approximately "complete" the data of each level of the uncarried out experiment, and then obtain the global optimal parameters [27].

By adjusting kernel functions and regularization parameters, SVM method can map complex nonlinear fitting problems to linear problems in high-dimensional space and approach arbitrary nonlinear functions, so it is widely used in small sample modeling[28]. LS-SVM not only inherits the good performance of SVM, but also changes the inequality constraints of SVM into equality constraints, and transforms the convex quadratic programming when solving Lagrange multipliers into linear equations, which greatly facilitates the solving process[29]. For a series of samples (x_i, y_i) , $i=1,2,3,\dots,n$. Where x_i is a m dimensional sample, $x_i \in R^m$ and y_i is the output vector, $y_i \in R$. Typically, the SVM output equation can be expressed as follows:

$$y = \sum_{i=1}^n w_i \Phi(x) + b \tag{17}$$

Where $b, w, \Phi(\square)$ is the bias term, the weight matrix and the nonlinear function respectively. Based on the SVM constraint condition, the error variable e_i is introduced into each sample, and the L2 regular term of the error variable is added to the original function. The constraint condition of LS-SVM is obtained as follows:

$$\begin{cases} \min_{w,b,e} J(w, e) = \frac{1}{2} w^T w + \frac{1}{2} C \sum_{i=1}^N e_i^2 \\ s.t. \quad y_i = w^T \varphi(x_i) + b + e_i, i = 1, \dots, N \end{cases} \tag{18}$$

Where c is the penalty parameter. For the nonlinear separable training samples, the original samples can be mapped to a higher-dimensional linearly separable space. The optimization problem of LS-SVM is a quadratic programming problem with equality constraints. The Lagrangian multiplier method is used to transform the original problem into a dual problem with a single parameter:

$$L(w, b, e, \alpha) = J(w, e) - \sum_{i=1}^N \alpha_i \{w^T \varphi(x_i) - b - y_i + e_i\} \tag{19}$$

Where α_i represents the Lagrange multiplier corresponding to x_i . Derive each variable of the Lagrange function according to the Karush-Kuhn-Tucker condition, and make the derivative zero:

$$\begin{cases} \frac{\partial L}{\partial w} = 0 \rightarrow w = \sum_{i=1}^N \alpha_i \varphi(x_i) \\ \frac{\partial L}{\partial b} = 0 \rightarrow \sum_{i=1}^N \alpha_i = 0 \\ \frac{\partial L}{\partial e_i} = 0 \rightarrow \alpha_i = C e_i, i = 1, \dots, N \\ \frac{\partial L}{\partial \alpha_i} = 0 \rightarrow w^T \varphi(x_i) + b - y_i + e_i = 0, i = 1, \dots, N \end{cases} \tag{20}$$

The support vector α and bias term b can be obtained from the equations set (20), and the final equation of LS-SVM can be expressed as follows:

$$\hat{y}_i = \sum_{i=1}^n \alpha_i K(x, x_i) + b \tag{21}$$

Where the kernel matrix is as follows:

$$\begin{aligned} \Omega_{il} &= \varphi(x_i)^T \varphi(x_l) \\ &= K(x_i, x_l), i, l = 1, \dots, N \end{aligned} \tag{22}$$

The radial basis function is selected as the kernel function as follows:

$$K(x, x_i) = \exp[-\|x - x_i\|^2 / 2\sigma^2] \tag{23}$$

The performance of the model depends on the penalty parameter c and kernel function parameters σ . In this paper, a simple and effective grid method[30,31] is used to optimize these parameters.

The four factors involved in the orthogonal experiment: the outer membrane thickness A, the outer membrane ion concentration B, the inner membrane thickness C, the inner membrane ion concentration D were selected as the model input, $x = \{A, B, C, D\}$, while the slope and the detection limit were respectively selected as the output y_i of the LS-SVM prediction model. Before establishing the model, it is necessary to preprocess the data to prevent the imbalance of weight allocation from causing the model overfitting. The commonly used data preprocessing method is normalization, however, in practical application, normalization will also compress the abnormal values in the sample to the prescribed range, which will affect the model training. In this paper, standardization is used for data preprocessing because most of the data obeys normal distribution, and for the loss function with regularized parameters, data standardization is also an excellent choice. The model standardization equation is as follows:

$$x' = \frac{(x_j - \bar{x}_j)}{S_j} \tag{24}$$

Where \bar{x}_j is the arithmetic mean of a feature and S_j is the standard deviation of that feature. The grid method is used to search the penalty parameter c in the error function and the kernel function parameter σ in the regions of $[0,0.1,100]$ and $[0,0.1,100]$, respectively. The penalty parameter c represents the degree of "punishment" beyond the error range, which can reduce the test error, prevent the model from overfitting, and reduce the complexity of the model. The grid search method can find the optimal combination under the condition of a given step size, and the quality of the model can be estimated by the following equation:

$$RMSE = \sqrt{\frac{1}{n} \sum_{i=1}^n (t_i - y_i)^2} \tag{25}$$

Where t_i is the true value and y_i is the predicted value. The final equation of the model can be written as:

$$\hat{y}_i = \sum_{i=1}^n \alpha_i K(x, x_i) + b = \sum_{i=1}^n \alpha_i \exp[-\|x - x_i\|^2 / 2\sigma^2] + b, \quad i = 1, \dots, 9 \tag{26}$$

For the slope prediction model, the RMSE is 0.00019 and the optimal parameter combination is:

$$[C, \sigma] = [25.9, 2.4] \quad ; \quad \alpha_i = [0.9176, -0.8876, 0.8858, 0.4306, 0.9129, -2.2593, 6.5982, -4.9116, 5.6919] \quad ,$$

$$b = -0.2313$$

For the detection limit prediction model, the RMSE is 0.00011 and the optimal parameter combination is:

$$[C, \sigma] = [49.5, 2.8] \quad , \quad \alpha_i = [0.2083, -0.6193, 1.6430, -3.2380, 1.2003, 0.8056, -4.6740, 1.1011, -8.3536] \quad ,$$

$$b = -0.0028$$

3.5. Membrane parameters optimization using the prediction model

In order to further find the optimal range of ion exchanger concentration and membrane thickness in the inner and outer layer, and improve the performance of the electrode, a prediction

model was established by LS-SVM, and the effects of those factors on the performance of the electrode were analyzed. The slope of the electrode is the most concerned parameter. When the slope is close to the Nernst slope, the lower the detection limit, the better. The results of orthogonal experiments show that the two factors of B and C are the main factors affecting the slope of the electrode, so A and D are selected as the fixed factors at the middle level (50 μm , 8.5 mol/m^3). According to the LS-SVM model of the slope of the electrode, the effects of factors B and C and their interaction on the slope of the electrode are obtained. 3D surface map and its 2D, 3D contour maps, as shown in the Fig.3.

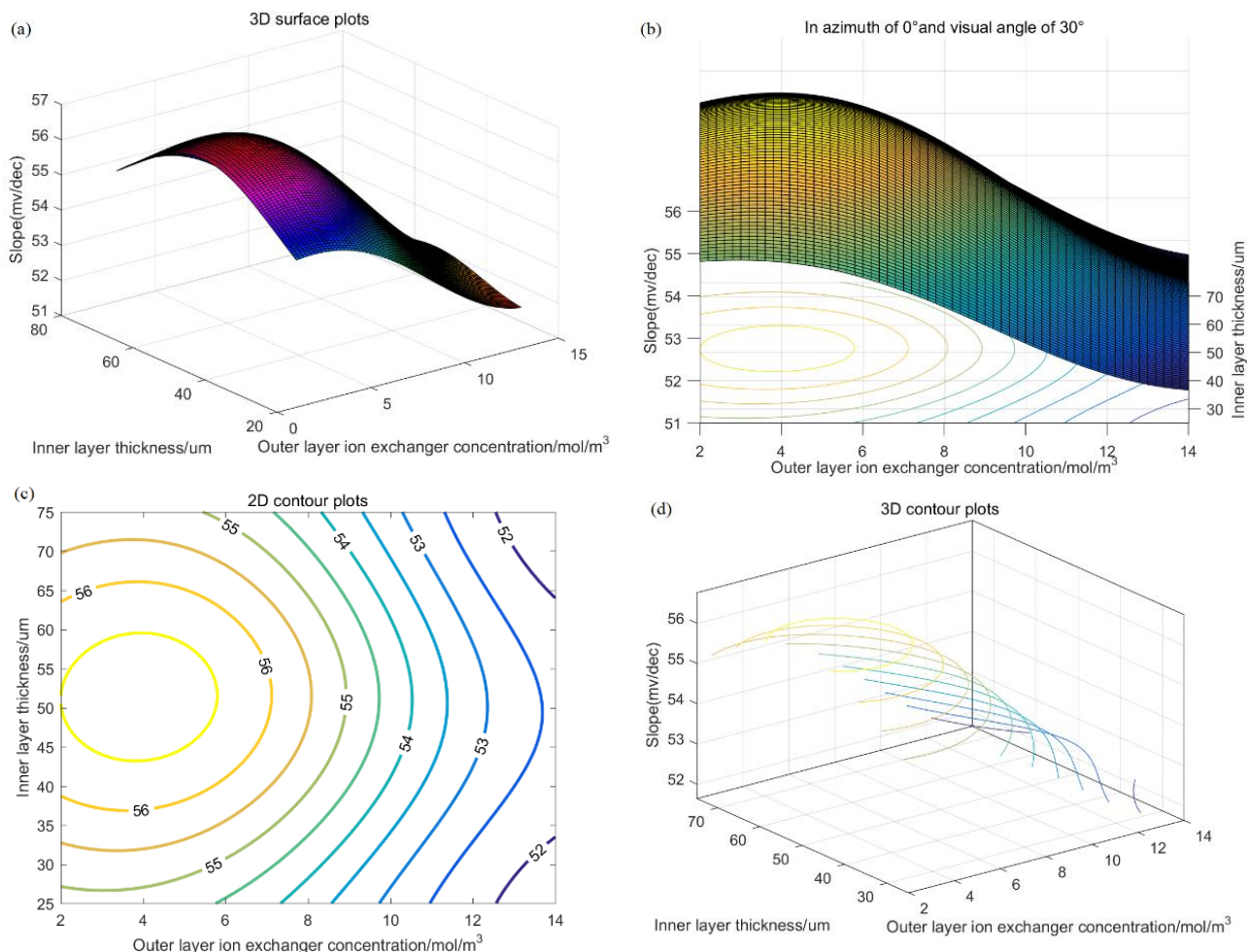


Figure 3. Effect of outer layer ion exchanger concentration and inner layer thickness on electrode slope (a) 3D surface plots, (b) Observation of Fig. 3 (a) in azimuth of 0° and visual angle of 30°, (c) 2D contour plots, (d) 3D contour plots.

It can be seen from the figure that the slope of the electrode is the largest when the thickness of the inner layer membrane is 45 to 60 μm , however, the change of the membrane thickness will only lead to the change of the slope of 2mV/dec. In the other hand, the slope of the electrode is more sensitive to the outer layer ion exchanger concentration. Different from the monolayer electrode, the slope of the electrode decreases with the increase of the outer layer ion exchanger concentration. In order to explain this phenomenon, the ratio of the outer layer ion exchanger to the inner layer ion exchanger is selected as a new factor to replace the concentration of the outer layer ion exchanger, and

the inner membrane thickness is maintained as another factor to re-establish the prediction model, as shown in Fig. 4.

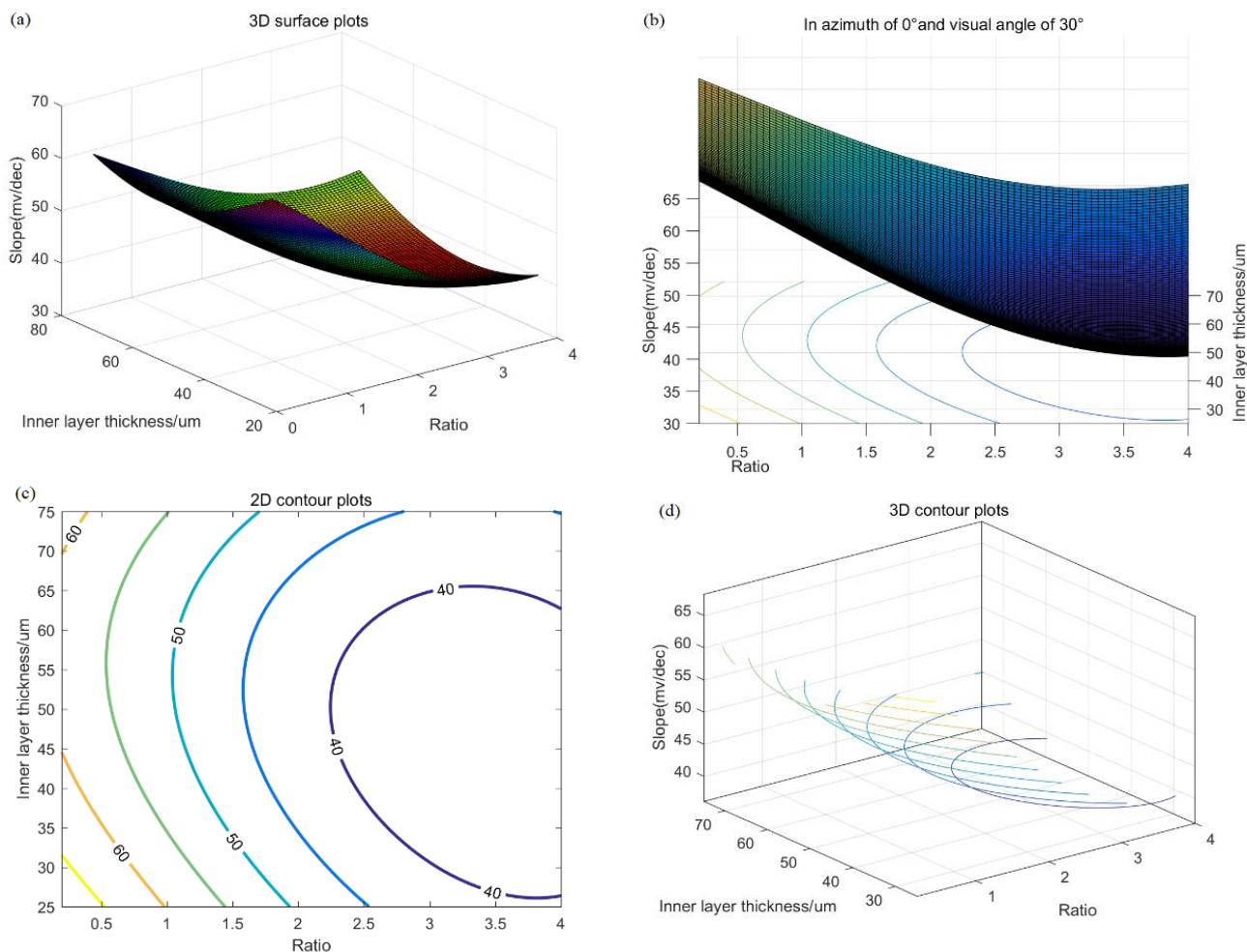


Figure 4. Effect of ion exchanger concentration ratio (outer/inner) and inner layer thickness on electrode slope (a) 3D surface plots, (b) Observation of Fig. 4 (a) in azimuth of 0° and visual angle of 30°, (c) 2D contour plots, (d) 3D contour plots.

As can be seen from Fig. 4, the trend of the effect of the inner membrane thickness on the electrode slope is similar to that before, and the medium thickness membrane is easier to obtain higher electrode slope. After using the concentration ratio of the outer layer ion exchanger to the inner ion exchanger as the input of the model, the effect of ion concentration on the electrode slope is further magnified, and the electrode slope changes greatly with the concentration ratio. When the concentration ratio is 4, the slope of the electrode is only 40mV. When the concentration ratio is less than 0.25, the electrode even has a slight super Nernst phenomenon. This shows that the difference of ion concentration between the inner and outer layers may have a significant effect on the ion flux and further affect the performance of the electrode. At the same time, it also explains why the electrode slope is better when the concentration of the outer layer ion exchanger is low. Combined with the results of Fig. 3 and Fig. 4, it is considered that the optimum range of inner layer membrane thickness is 45 to 65 μm, the optimum range of outer layer ion concentration is 2 to 6 mol/m³, and the concentration ratio is about 0.25.

For the detection limit of the electrode, two factors C and D with a larger range in the orthogonal experiment are also selected to establish the prediction model, and the other two factors A and B are selected as the fixed factors at the middle level (50 μ m, 8.5 mol/m³). According to the LS-SVM model of the detection limit of the electrode, the effects of factors C and D and their interaction on the slope of the electrode are obtained. 3D surface map and its 2D, 3D contour maps, as shown in the Fig.5.

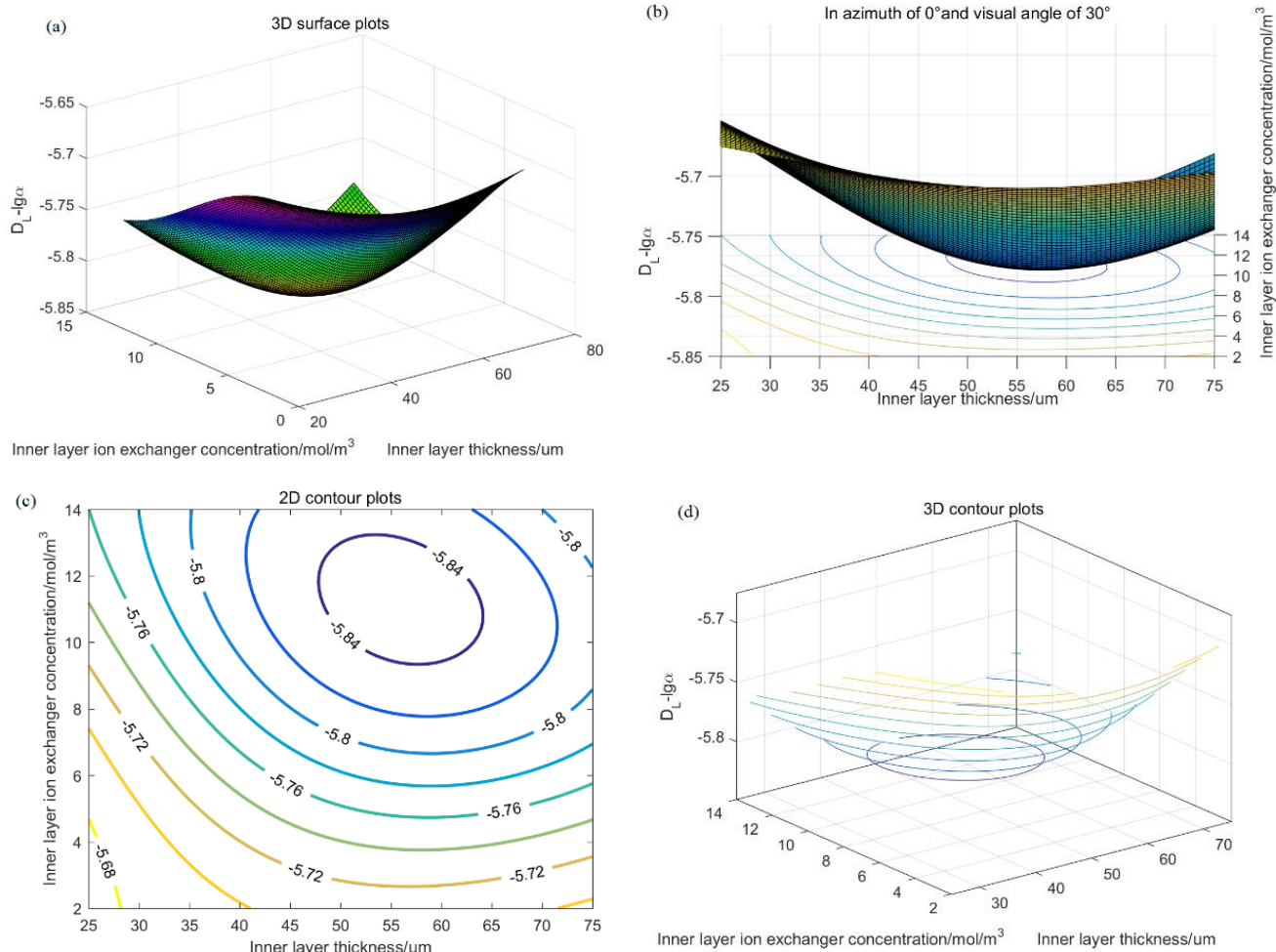


Figure 5. Effect of inner layer ion exchanger concentration and inner layer thickness on electrode detection limit (a) 3D surface plots, (b) Observation of Fig .5 (a) in azimuth of 0° and visual angle of 30°, (c) 2D contour plots, (d) 3D contour plots.

It can be seen from Fig. 5 that the detection limit is affected by the change of the ion concentration in the inner layer. With the increase of the ion concentration in the inner layer, the detection limit of the electrode decreases gradually, and the detection limit reaches the lowest when the ion concentration in the inner layer is 9 to 13 mol/m³. The thickness of the membrane also affects the detection limit. With the increase of the thickness of the inner layer, the detection limit of the electrode decreases gradually, until the thickness of the inner film is 50 to 65 μ m, the detection limit reaches the lowest. This may be due to the fact that the ion flux variation region is concentrated on both sides of the membrane junction, and the ion concentration will significantly affect the ion flux in the transition

region, while the ion concentration in the deep layer of the membrane far from the interface is almost the same. The continued increase of membrane thickness will not continue to have a significant effect on ion flux.

In the two groups of orthogonal experiments, the range of outer layer membrane thickness is almost the lowest. In order to determine the optimal value range, factors A and D are selected as model variables, B and C are selected as the fixed factors at the middle level (50 μm , 8.5 mol/m³), and the result is shown in Fig. 6.

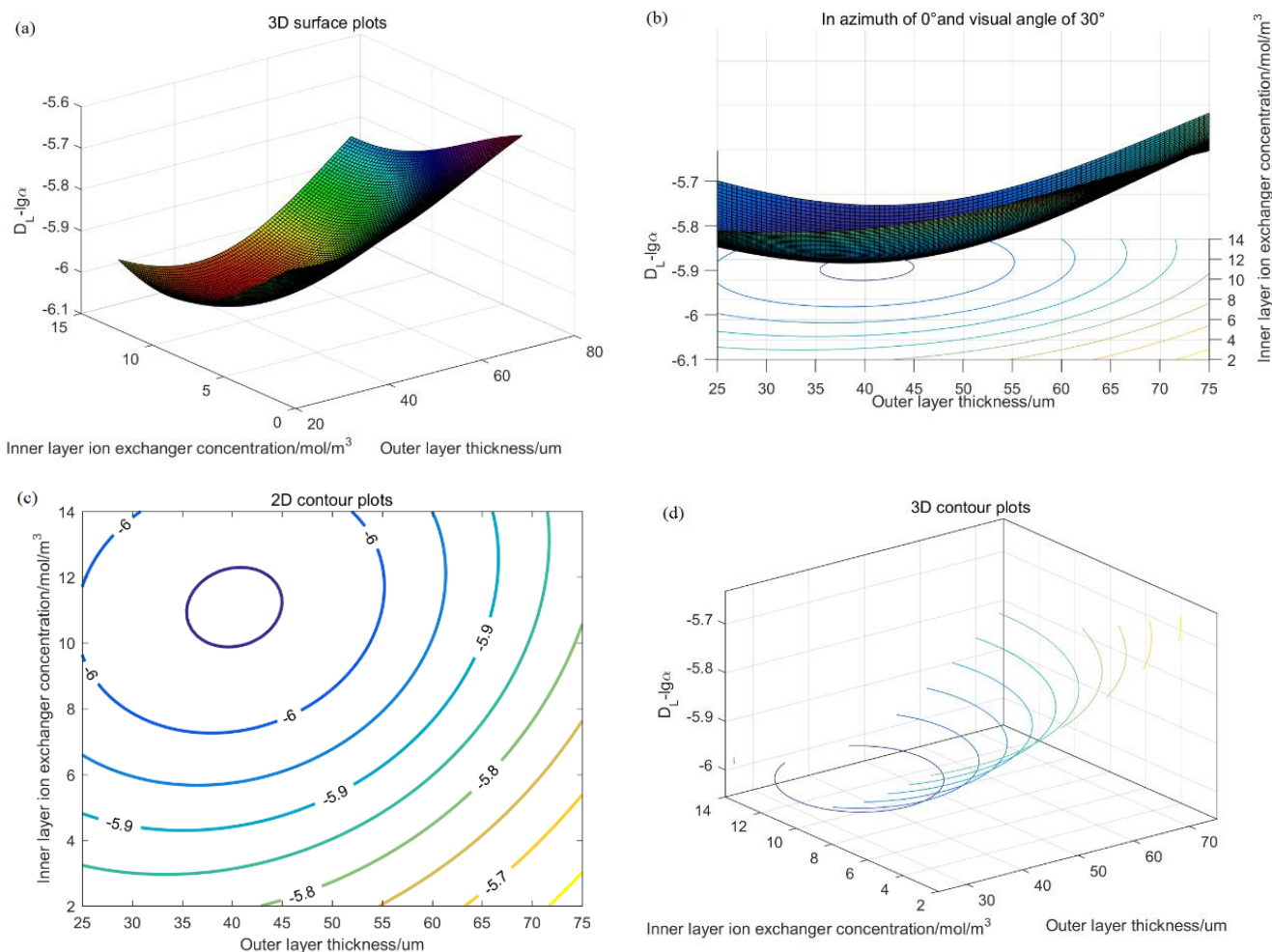


Figure 6. Effect of inner layer ion exchanger concentration and outer layer thickness on electrode detection limit (a) 3D surface plots, (b) Observation of Fig. 6 (a) in azimuth of 0° and visual angle of 30°, (c) 2D contour plots, (d) 3D contour plots.

It can be seen from Fig 6 that the detection limit of the electrode reaches the lowest in the inner concentration 10 to 12 mol/m³, which is consistent with the results obtained by the model of Fig 5. The optimal range of the thickness of the outer layer membrane is 35 to 45 μm , which is exactly between the first level and the second level of the orthogonal experiment. This shows that after ensuring that the transition region on both sides of the solution-outer layer membrane interface and the outer layer-inner layer membrane interface are not intersect, the thickness of the outer layer should be as thin as possible.

By selecting the intersection of the optimal regions obtained by the four groups of models one by one, and selecting the midpoint of the intersection as the optimal value of this factor, the optimal values of the four factors can be obtained: outer layer thickness 40 μm , outer layer ion exchanger concentration 2.75 mol/m^3 , inner layer thickness 52.5 μm and inner layer ion exchanger concentration 11 mol/m^3 .

3.6. Potentiometric calibration plots

According to the optimal parameters given by the model, three electrodes were made according to the same process. The parameters of ion concentration and thickness of the inner layer were substituted into the bicarbonate ion exchange model, and the soaking time was 393 s. Finally, the electrode was tested in sodium chloride solution and the calibration curve was obtained. The No. 9 electrode of the orthogonal experiment is selected as the comparison, and the final result is shown in Fig. 7. It can be seen from the figure that the optimal parameters obtained by the model further improve the performance of the electrode. The average slope of the electrode is 58.7 mV/dec . When the ion concentration is lower than 10^{-6} mol, the slope of the electrode decreases, but the decrease is smaller than that of the No. 9 electrode, which is 25 mV . When the concentration is lower than 10^{-7} mol, the electrode can hardly distinguish the change of solution concentration, and the final detection limit is $10^{-6.5}$ mol.

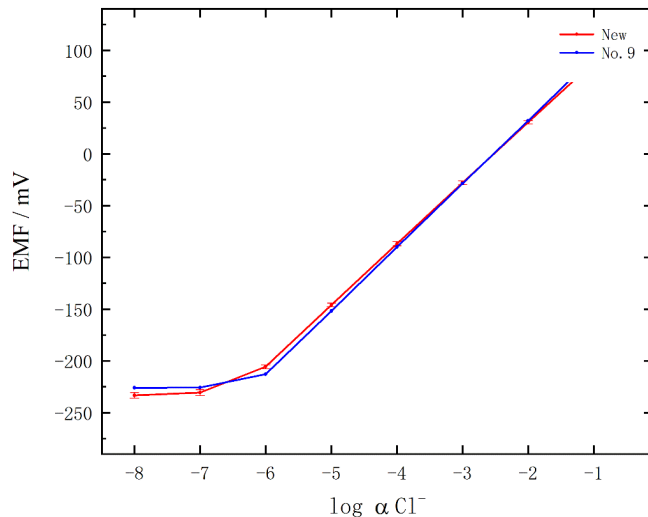


Figure 7. Potentiometric calibration plots for optimized electrode (red) in LS-SVM model and No. 9 electrode in orthogonal experiment (blue).

Compared with other monolayer chloride ion selective electrodes, whether liquid or solid contact, bilayer membrane chloride ion electrode shows a better potential response. As shown in Table 5, the linear range of bilayer membrane chloride ion electrode is the largest of all electrodes, and the detection limit is the lowest of all electrodes, which provide that the detection performance of bilayer membrane chloride ion electrode optimized by LS-SVM have been effectively improved.

Table 5. Comparison of polymeric membrane chloride ion-selective electrodes.

Electrode	Slope (mV/decade)	Linear range (M)	Detection limit (M)	Linearity (R^2)	Reference
Liquid filled electrode	56.9mV	$10^{-5} - 10^{-1}$	1×10^{-5}	-	[16]
Indium Tin Oxide Glass electrode	54.0mV	$10^{-4} - 10^{-1}$	8×10^{-5}	0.990	[32]
Solid contact electrode	58.1mV	$10^{-4} - 10^{-1}$	1×10^{-5}	0.999	[33]
Microfluidic sensor	64.6mV	$10^{-5} - 10^{-1}$	1×10^{-5}	0.972	[19]
Bilayer membrane electrode	58.7mV	$10^{-6} - 10^{-1}$	$1 \times 10^{-6.5}$	0.997	This work

3.7. Real sample test

In order to evaluate whether the optimized bilayer membrane chloride electrode can meet the requirements of real sample measurement, the real sample test of the electrode was carried out. The real samples used in this test were collected from tap water treated by ultrafiltration and secondary reverse osmosis. After sampling, the real samples were stored in an airtight container and different quality of sodium chloride was added systematically. The experimental results in Table 6 show that the recoveries were from 99.9% to 103.2%, indicating that the electrode is sensitive to chloride ion in both laboratory and actual water sample analysis.

Table 6. Determination of Cl^- in real samples

Samples	Added (mM)	Expected (mM)	Found (mM)	Recovery (%)
1	0		0.0087	-
2	0.01	0.0187	0.0193	103.2
3	0.02	0.0387	0.0393	101.6
4	0.05	0.0887	0.0895	100.9
5	0.1	0.1887	0.1886	99.9

4. CONCLUSIONS

In this work, a bilayer membrane chloride ion electrode was designed and fabricated. The electrode membrane is based on PVC, while the inner layer and outer layer have two different ion exchangers TDMACl and TDMAHCO₃. The ion exchange time of the inner membrane was determined by finite difference simulation method. The orthogonal experiment based on the thickness and ion exchanger concentration of inner and outer membrane was designed, and the electrode performance prediction model was established by taking these factors as LS-SVM input, electrode slope and detection limit as output, and the optimal parameters of electrode factors were obtained. According to the model, changing the concentration of the inner and outer ion exchanger can significantly change the ion flux and then change the slope and detection limit of the electrode, and changing the thickness of the inner membrane can reduce the detection limit of the electrode, while the

thickness of the outer membrane has little effect on the performance of the electrode. Through the verification experiment, the slope of the new electrode is 58.7 mV/dec and the detection limit is $10^{-6.5}$ mol. The bilayer membrane structure is suitable not only for acrylic cationic electrodes, but also for PVC materials and anions. Compared with the monolayer membrane electrode, the bilayer membrane electrode has more variable parameters. Parameter modeling is the best way to optimize these complex factors. Therefore, the combination of bilayer membrane and modeling optimization can maximize the performance of the electrode and make the polymer membrane electrode more widely used.

ACKNOWLEDGEMENTS

This work was supported by the National Natural Science Foundation of China (No.61771034).

References

1. N. Pankratova, M. Cuartero, L. A. Jowett, E. N. W. Howe, P. A. Gale, E. Bakker and G. A. Crespo, *Biosens. Bioelectron.*, 99 (2018) 70.
2. S. Cinti, L. Fiore, R. Massoud, C. Cortese, D. Moscone, G. Palleschi and F. Arduini, *Talanta*, 179 (2018) 186.
3. C. Cheng, Z. M. Huang, W. Y. Chung, D. G. Pijanowskad and M. Dawgul, *J. Chin. Chem. Soc.*, 59 (2012) 122.
4. Q. Yuan, C. Shi, G. De Schutter, K. Audenaert and D. Deng, *Constr. Build. Mater.*, 23 (2009) 1.
5. R. Zielińska, E. Mulik, A. Michalska, S. Achmatowicz and M. Maj-Żurawska, *Anal. Chim. Acta*, 451 (2002) 243.
6. B. N. Biswas, M. Y. A. Mollah and M. A. B. H. Susan, *Ionics*, 18 (2011) 189.
7. E. McCafferty, *Corros. Sci.*, 45 (2003) 1421.
8. A. Munis, M. Zheng and T. Zhao, *Mater. Res. Express*, 6 (2019) 076541.
9. P. Vainikka, D. Bankiewicz, A. Frantsi, J. Silvennoinen, J. Hannula, P. Yrjas and M. Hupa, *Fuel*, 90 (2011) 2055.
10. D. Bankiewicz, P. Vainikka, D. Lindberg, A. Frantsi, J. Silvennoinen, P. Yrjas and M. Hupa, *Fuel*, 94 (2012) 240.
11. G. Williams and H. N. McMurray, *Corrosion*, 62 (2006) 231.
12. Y. Noguchi, L. Zhang, T. Maruta, T. Yamane and N. Kiba, *Anal. Chim. Acta*, 640 (2009) 106.
13. M. M. Watt, J. M. Engle, K. C. Fairley, T. E. Robitshek, M. M. Haley and D. W. Johnson, *Org. Biomol. Chem.*, 13 (2015) 4266.
14. R. Zhang, S. Xu, Y. Zhu, J. Luo, X. Liu and D. Tang, *Colloid Polym. Sci.*, 294 (2016) 1643.
15. A. Kisiel, A. Michalska and K. Maksymiuk, *J. Electroanal. Chem.*, 766 (2016) 128.
16. M. Rothmaier, U. Schaller, W. E. Morf and E. Pretsch, *Anal. Chim. Acta*, 327 (1996) 17.
17. P. Sjöberg-Eerola, J. Bobacka, A. Lewenstam and A. Ivaska, *Sensor. Actua.B-Chem.*, 127 (2007) 545.
18. S. C. Tseng, T. Y. Wu, J. C. Chou, Y. H. Liao, C. H. Lai, J. S. Chen, S. J. Yan, M. S. Huang, T. W. Tseng and Y. H. Nien, *Mater. Res. Bull.*, 101 (2018) 155.
19. J. C. Chou, T. W. Tseng, Y. H. Liao, C. H. Lai, S. J. Yan, Y. X. Wu, C. Y. Wu and S. H. Lin, *IEEE Sens.J.*, 19 (2019) 3217.
20. M. Lyczewska, M. Wojciechowski, E. Bulska, E. A. H. Hall, K. Maksymiuk and A. Michalska, *Electroanalysis*, 19 (2007) 393.

21. A. Kisiel, E. Woźnica, M. Wojciechowski, E. Bulska, K. Maksymiuk and A. Michalska, *Sensor. Actua.B-Chem.*, 207 (2015) 995.
22. K. Farhadi, M. Bahram, D. Shokatynia and F. Salehiyan, *Talanta*, 76 (2008) 320.
23. S. Y. Kazemi, A. Hamidi, N. Asanjarani and J. Zolgharnein, *Talanta*, 81 (2010) 1681.
24. C. Dong and J. Chen, *Bioresour. Technol.*, 271 (2019) 174.
25. S. Dabrowska, J. Migdalski and A. Lewenstam, *Electroanalysis*, 29 (2017) 140.
26. W. E. Morf, E. Pretsch and N. F. De Rooij, *J. Electroanal. Chem.*, 602 (2007) 43.
27. G. B. Huang, H. Zhou, X. Ding and R. Zhang, *IEEE Trans.Syst.Man.Cybern.*, 42 (2012) 513.
28. Z. Liu, L. Wang, Y. Zhang and C. L. P. Chen, *Appl.Soft.Comput.*, 38 (2016) 738.
29. Q. Xiao, X. Bai and Y. He, *Foods*, 9 (2020) 94.
30. T. Hacib, Y. Le Bihan, M. R. Mekideche, H. Acikgoz, O. Meyer and L. Pichon, *IEEE Trans. Magn.*, 46 (2010) 2811.
31. M. I. Mukarev and K. B. Walsh, *J.Near.Infrared.Spec.*, 20 (2012) 647.
32. J. F. Cheng, J. C. Chou, T. P. Sun, S. K. Hsiung and H. L. Kao, *Jpn.J. Appl.Phy.*, 50 (2011) 037001.
33. Z. Li, M. Lei and J. Chen, *Int. J. Electrochem. Sci.*, (2017) 11715.

© 2020 The Authors. Published by ESG (www.electrochemsci.org). This article is an open access article distributed under the terms and conditions of the Creative Commons Attribution license (<http://creativecommons.org/licenses/by/4.0/>).